frontiers | Frontiers in Astronomy and Space Sciences

TYPE Mini Review
PUBLISHED 21 June 2024
DOI 10.3389/fspas.2024.1401797

OPEN ACCESS

EDITED BY
Gianluca Calcagni,
Spanish National Research Council (CSIC), Spain

REVIEWED BY
Fabrizio Fiore,
National Institute of Astrophysics (INAF), Italy
Francesco Tombesi,
University of Rome Tor Vergata, Italy

*CORRESPONDENCE
Demosthenes Kazanas,
demos.kazanas@nasa.gov

RECEIVED 16 March 2024
ACCEPTED 13 May 2024
PUBLISHED 21 June 2024

CITATION
Kazanas D (2024), Active galactic nuclei: global perspective and time-domain implications.
Front. Astron. Space Sci. 11:1401797.
doi: 10.3389/fspas.2024.1401797

Active galactic nuclei: global perspective and time-domain implications

Demosthenes Kazanas*

NASA, Goddard Space Flight Center, Greenbelt, MD, United States

A view of the global structure of active galactic nuclei (AGN) is presented herein following the detection of blue-shifted warm absorber (WA) and ultrafast outflow (UFO) absorption features in their X-ray spectra. A straightforward interpretation of these features suggests the presence of magnetohydrodynamic winds off the underlying accretion disks spanning a wide range of a few to ~10^6 Schwarzschild radii. UFOs are associated with wind segments closest to a black hole, with decreasing ionization absorber species associated with these wind segments at increasingly larger distances; eventually, the wind segments at the largest distances are sufficiently cool and dusty to be associated with the AGN tori, as suggested in the past. Furthermore, spectroscopic X-ray observations at a sufficient resolution allow estimates of the mass fluxes of these winds, showing that they increase with radius. As a consequence, the mass flux of the underlying accretion disk must decrease toward the accreting black hole, eventually reaching a value smaller than that needed to convert the flow into an X-ray hot advection-dominated accretion flow; it is suggested that this hot segment of the accretion flow is responsible for the observed AGN X-rays (and galactic X-ray binaries) in place of the *ad hoc* corona assumed thus far. This work indicates that the properties of this component that are reflected in its relative luminosity to the viscous disk O-UV component depend on the source luminosity in broad agreement with the observations.

KEYWORDS

black hole, accretion, accretion disks, magnetohydrodynamic wind, active galactic nuclei

1 Introduction: main components of the spectral energy distribution of active galactic nuclei

Sixty years after their discovery, quasars and more broadly active galactic nuclei (AGN) continue to puzzle scientists. Although observational and theoretical advancements over the years have sharpened our views regarding these objects, a comprehensive, low-parameter picture of their associated structures and properties is lacking. Following the discovery of quasars and their association with luminous radio sources, it was shown early on that the efficiency of their radiation must be higher than that of nuclear burning; as such, they are likely powered by the more efficient process of matter accretion onto a black hole (Lynden-Bell, 1969), likely though dissipation in an accretion disk. Following this, the seminal work on accretion disks and their spectral appearance was developed by Shakura and Sunyaev (1973) (hereafter SS73; see also Kubota and Done (2018) for more recent models).

The accretion disks described in SS73 have steady states and generally thin geometric structures that are in vertical hydrostatic equilibrium with azimuthal velocities

much higher than the poloidal and radial velocities ($V_\phi \gg V_z > V_r$). Matter sinks slowly toward a black hole, transferring its angular momentum outward, while locally dissipating the fraction of its kinetic energy released from infinity in addition to that transferred outward along the smaller radii with the angular momentum. The dissipated energy along the radius r, given approximately by $\dot{E} \simeq GM\dot{M}/r$, is considered to be emitted in the black body form of temperature T, such that $\sigma T^4 = 3GM\dot{M}/(8\pi r^3)$ (the factor $(3/8\pi)$ results from including both the energy released from infinity to r and that transferred outward by the viscous stresses; Novikov and Thorne (1973); Shapiro and Teukolsky (1986); Frank et al. (1985)). The resulting spectrum is then a superposition of the black-body spectra of radial temperature dependence $T \propto r^{-3/4}$.

This results in a feature broader than that of a single black body with luminosity per logarithmic frequency $\nu L_\nu \propto \nu^{4/3}$, maximum temperature set by the accretion rate $\dot{M}$, and black hole mass M (in reality by the value of the innermost stable circular orbit (ISCO); $R_{ISCO} \simeq 2-6M$ depending on the value of the black hole spin). This feature is commonly referred to as the big blue bump (BBB) because it dominates the overall emission and peaks in the ultraviolet (UV) region of the electromagnetic spectrum in most quasars.

By introducing the value of the Eddington accretion rate $\dot{M}_E = L_E/c^2$, where L_E is the Eddington luminosity given by $L_E \simeq 1.3 \times 10^{46} M_8 \mathrm{erg/s} (M_8 = (M/10^8 M_\odot))$, and the normalized accretion rate $m = \dot{M}/\dot{M}_E$, the maximum temperature associated with the BBB is obtained as $T \simeq 10^5 (\dot{m}/M_8)^{1/4} = 10^7 (\dot{m}/M_1)^{1/4}$. For AGN with high luminosity and masses in the range of 10^8–$10^9 M_\odot$, this feature peaks in the UV part of the spectrum; for galactic accreting black holes of mass only a few solar masses, this feature peaks in the soft X-ray spectral band, in agreement with observations.

Additional observations have shown that aside from the above multitemperature black-body feature, the spectra of accreting black holes almost universally include harder (> 2 keV) X-rays (with exceptions being the tidal disruption events (TDEs) that exhibit very little emissions above $E > 2$ keV); these are generally in the accordance with a power law with the photon spectra $dN/dE \propto E^{-\Gamma}$ with $\Gamma \sim 1.5$–2.5 and an (apparent whenever it is detected) exponential cut-off at $E \sim 50$–100 keV. The origin of this higher energy component is attributed to an *ad hoc* hot ($T_e \sim 10^9$ K) corona, which produces the observed X-rays by Comptonization of the disk photons through the hot electrons. The properties of the corona (electron temperature T_e, Thomson depth τ and geometry, and resulting luminosity) are not given *a priori* but are chosen so as to account for specific observations.

In addition to their X-ray and O-UV continua, the AGN spectra exhibit prominent line emissions. These comprise two general groups, i.e., broad permitted lines (typically of $\Delta V \sim 10,000$ km/s) such as C IV, Lyα, N V, Mg II, Hα, and Hβ as well as narrow and typically forbidden lines ($\Delta V \sim 2,000$ km/s) such as O III. It is generally considered that the line velocities represent the dynamics of the plasma emissions in the gravitational field of a black hole, implying that the broad lines are emitted closer to the gravitating object than the narrow ones. The issues of their origin as well as physical, kinematic, and dynamic properties have been the subjects of numerous studies, resulting in several interesting correlations (Sulentic et al., 2000, 2017) whose origins are not yet firmly established. To further increase the AGN diversity, a large proportion of them exhibit narrow permitted lines, thereby producing two line-based categories as type 1 (broad permitted lines) and type 2 (narrow permitted lines).

Observations of the type 2 AGN (Seyfert 2 galaxies) in polarized light have shown the existence of broad line components; however, these are observed only in polarized light, suggesting that their broader component closer to the AGN center is blocked from direct view by a structure of significant height-to-radius (h/r) ratio. The properties of this component indicated a cold, potentially dusty/molecular structure of toroidal shape called the "AGN torus"; this feature was then added as one of the important components of AGN phenomenology (Antonucci, 1993). The dusty, molecular make-up of these tori implies that they must be cool ($T \sim 10$–100 K) structures that do not produce their own radiation but apparently intercept and reprocess a large fraction of the AGN UV and X-rays into infrared (IR) rays. The major problem with this notion is their large h/r ratios given their low temperatures compared to the local virial ones with temperatures $\gtrsim 10^7$ K. Although these tori are hailed as the crux of the unification of types 1 and 2 AGN, further observations over the years appear have indicated a more complex structure (Netzer, 2015).

Finally, in addition to the X-ray to far-infrared (FIR) spectral components that are attributed to features associated with their accretion disks (which we are unable to resolve spatially), AGN are invariably detected at radio frequencies (~1 GHz). These emissions are generally associated with largely resolvable, ubiquitous jets that apparently originate near the AGN centers and span distances of the order of parsecs to megaparsecs. Interestingly, the radio emissions vary widely among the different AGN as a fraction of their bolometric luminosity; despite the small values of these fractions ($L_r/L_{bol} \sim 10^{-3} - 10^{-6}$), they are employed as yet another discriminator to separate the classes. Hence, depending on the value of this ratio, the AGN are distinguished as radio loud (RL) ($L_r/L_{bol} \sim 10^{-3}$) and radio quiet (RQ) ($L_r/L_{bol} \sim 10^{-6}$). The radio flux of the RL AGN spectra connects smoothly with that of the FIR, contrary to that of the much weaker flux of the RQ AGN that appears completely separate (Figure 1). Furthermore, RL AGN have been detected by the Fermi-LAT at energies of $E_\gamma \simeq 10$ GeV and even tera electron volts on occasion, and the γ-ray flux dominates the entire spectral energy distribution (SED) in many cases (Figure 1B). This feature, along with the differences in their L_r/L_{bol} ratios, imply that RL AGN are endowed with additional non-thermal components aside from those that produce the FIR to X-ray spectra, which are absent in the RQ AGN.

Based on these multiwavelength facts, it is interesting to put together an all-inclusive AGN scheme, such as the well-known one by Urry and Padovani (1995) shown in Figure 1 and its variations. Although this may be useful in providing a broad picture of the AGN, it has little reference to the underlying physics. Clearly, the AGN are multiwavelength, multiscale objects presenting observers with a multitude of facts even for a relatively narrow frequency band that roughly spans one decade (e.g., see the recent review by Netzer (2015)). Although each of these sets is important in its own right to the specific subfield, the following questions need to be addressed: Are all facts equally important to the global AGN picture? Are the properties of a given spectral band independent of those of other bands or are they interrelated? Is there a small number parameter comprehension of the global AGN structure?. It is the goal of this

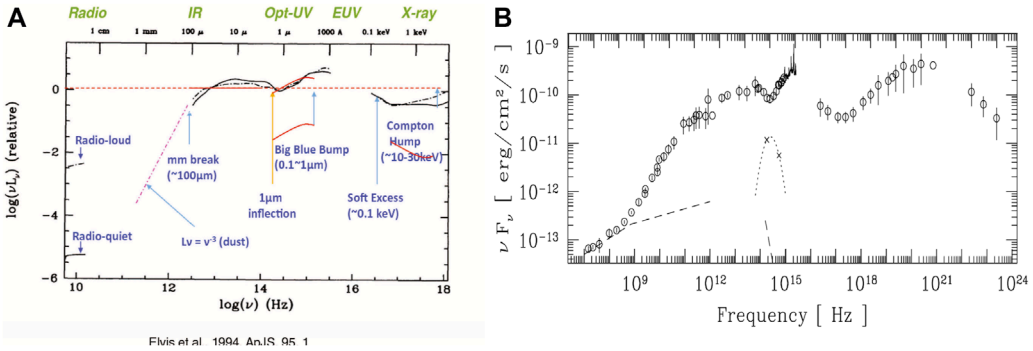

FIGURE 1
(A) General form of the AGN SEDs (both RL and RQ) from radio to X-ray frequencies. **(B)** SED of the RL AGN 3C 273, indicating continuous flux from radio to γ-ray range.

work to indicate the path to this global picture. To the best of the author's knowledge, the first attempt in this direction was the work of Boroson (2002), where principal component analysis (PCA) was employed on a set of 87 nearby RL and RQ AGN to formulate a 2D parametrization of the AGN according to their fractional Eddington luminosity values, L/L_E, and accretion rates $\dot{M}$. This analysis was driven by the radio loudness and also the properties of the Fe II[O III], He II, and Hβ components that were employed to provide estimates of the black hole mass. Although this analysis provides the global location of the AGN in the $L/L_E - \dot{M}$ diagram, insights concerning the relative importances of the individual spectral AGN bands are also important.

With respect to this last issue, considering that the AGN luminosity is driven by the black hole potential, it is expected that the contributions of the individual components would decrease with frequency, as implied by the spectral shape of the accretion disk. The fact that the FIR and line emissions have comparable luminosity values with the higher energy continuum determines that the former subtend a significant fraction of the latter's solid angle, thereby setting the structure of the large-scale AGN geometry.

This finding becomes more complicated with the relative contributions and geometries of the O-UV and X-ray components. Based on the models that assume the O-UV emissions to be caused by a disk (of the SS73 type or otherwise) that reaches the ISCO of the black hole, this broad and multicolor component should be dominant, as in the case of most AGN. As noted earlier, the X-ray emissions are attributed to the corona, whose geometry as well as spectral properties and luminosity in particular are typically chosen to fit the data. However, this picture has been challenged by microlensing observations; Morgan et al. (2010) showed that the X-ray emitting region was $\simeq 10$ times smaller than that of UV emissions, despite the fact that the BBB luminosity was larger than that for X-rays (i.e., the ratio $R_{UVX} = L_{BBB}/L_X > 1$), thereby violating the qualitative accretion disk rule that the smallest disk radii emit the most radiation. It is of additional interest that this ratio, which is usually presented as the logarithmic slope of the AGN flux between 2500 Å and 2 keV and referred to as $\alpha_{\rm OX}$, is not constant. Despite the complications of the overlying galaxy in the determination of the true BBB luminosity, $\alpha_{\rm OX}$ has been found to depend on the source luminosity at 2500 Å (Strateva et al., 2005), implying the presence of as yet incomprehensible physics that determines its value.

Significant insights may be obtained on the issue of the dependence of R_{UVX} values on the source luminosity from observations of galactic X-ray sources; these indicate that the ratio of fluxes between the multicolor black-body disk (their BBB equivalent) and power-law-based hard X-ray components depends on the source luminosity: at high values of the source luminosity, the spectrum is dominated by the multicolor quasithermal disk component, with the harder X-ray component being subdominant and having high energy spectral index values of $\Gamma > 2$. At lower source luminosities, the multicolor disk spectrum becomes subdominant with hard X-ray index values of $\Gamma < 2$, indicating that the same source can exist in two different states (Esin et al., 1997, 1998). A similar behavior in the AGN would then account for the results of Strateva et al. (2005) if the sources at the highest values of L_{UV}, which exhibit the most negative values of $\alpha_{\rm OX}$, have the highest Eddington ratios.

The following section provides a brief review of the scaling employed in relation to the broader class of accretion problems, along with some data that evidence the presence of magnetohydrodynamic (MHD) winds off the entire extent of the AGN accretion disks. Furthermore, the presence of these winds is shown to imply a decreasing disk accretion rate toward the black hole and its conversion to a hot advection-dominated accretion flow (ADAF) that accounts for the AGN X-ray emissions and their effects on the relative AGN UV and X-ray luminosities. Finally, the concluding section presents some general comments and observations regarding the overall AGN properties and future directions to be pursued for their deeper understanding.

2 AGN/X-ray binaries accretion disks and winds

2.1 Accretion/outflow unification along the mass scale

As discussed in Kazanas et al. (2012), for problems regarding accretion or winds in the gravitational field of a black hole, it

is convenient to normalized the radius by their Schwarzschild radius $x = r/r_S, r_S = 2GM/c^2 \simeq 3\times10^5 M_\odot$ cm, the luminosity by their Eddington luminosity $L_E \simeq 2\pi m_p c^3 (r_S/\sigma_T) \simeq 1.3\times10^{38} M_\odot$ erg/s (where m_p and σ_T are the proton mass and Thomson cross section, respectively), and the accretion rate by their corresponding Eddington rate, i.e., $\dot{m} = \dot{M}/\dot{M}_E$ (where $\dot{M}_E = L_E/c^2$). These scalings then indicate that as long as the flow velocities are proportional to the Keplerian ones $v \propto v_K = c(2x)^{-1/2}$, the Thomson depth of the flows τ is independent of the black hole mass and depends only on $\dot{m}$ and the dimensionless radius x, such that $\tau = r_S \sigma_T n_0 \simeq \dot{m}$ *for* $x \simeq 1$ with n_0 being the density normalization near the horizon. The universality of the X-ray properties of the AGN and galactic X-ray binaries, which involve mainly their Thomson depths, argues favorably for this point of view.

This scale invariance is broken by processes including absorption, the BBB disk emission, and AGN tori temperatures, whose properties scale with the black hole mass and x. The maximum temperature associated with the BBB, assuming $x \simeq 1$, is given by $T_{BBB} \simeq 10^5 (\dot{m}/M_8)^{1/4} = 10^7 (\dot{m}/M_1)^{1/4}$. For high-luminosity AGN with masses in the range of $10^8 M_\odot$ to $10^9 M_\odot$, this feature peaks in the UV part of the spectrum; for galactic accreting black holes of mass only a few solar masses, the feature peaks in the soft X-ray spectral band, in agreement with observations. Similarly, the tori temperatures scale as $T_{tor} \sim 300(\dot{m}/M_8^3)^{1/4} x_6^{-1/2}$ K, where $x_6 = (x/10^6)$.

For the BBB, X-rays, and their corresponding scalings that are in broad agreement with observations over the black hole mass range of eight decades, it is reasonable to consider that the accretion of a black hole can be studied along the accreting black hole mass scale using a reasonably small number of parameters. The tori temperatures are also in broad agreement with observations, but their luminosities depend on the physical characteristics; their apparent absence in the galactic X-ray sources depend on the sizes of their accretion disks, as discussed later.

2.2 Wind structure and ionization

One of the more significant discoveries of the ASCA, Chandra, and XMM-Newton is the presence of blue-shifted absorption features in the X-ray spectra of $\gtrsim 50\%$ of the AGN, whose origins lie in the photoionization of the outflowing plasma by the AGN continuum. The X-ray absorbers are of particular interest because of their wide range of ionization states (Fe XXVI to Fe II) and corresponding range of outflow velocities from $v \sim 300$–500 km/s (referred to as warm absorbers (WA) (Reynolds and Fabian, 1995)) to $v > 10{,}000$ km/s (referred to as ultrafast outflows (UFOs) (Tombesi et al., 2010)). A similar fraction of the AGN spectra was also found by the Hubble space telescope (HST) to exhibit UV absorbers (Crenshaw et al., 2003), indicating the ubiquitous presence of winds in accreting black holes.

2.2.1 Absorption measure distribution

The wide ranges of ionization states and velocities have prompted the consideration of different regions with various values for their ionization parameter $\xi = L_{ion}/n(r)r^2 = L_{ion}/N_H r$ (where L_{ion} and $n(r)$ are the ionizing luminosity and plasma density, respectively) and velocity v. In this respect, Holczer et al. (2007) and Behar (2009) offered a different approach: they assumed a continuous variation of the absorber equivalent width given by $N_H(r)$ as a function of the ionization parameter ξ, i.e., $N_H(r) \sim \xi^\alpha$, or more specifically what they called the absorption measure distribution, $AMD = dN_H/d\log\xi \propto \xi^\alpha$, to derive a value for the parameter α through a global fit of the values of N_H of the ions over a wide ξ range. Incidentally, by virtue of the definition of ξ, the AMD also implies a power-law range for the plasma density $n(r)$ along the line of sight (LoS) of the observer in the form $n(r) \propto r^{-s}$, with $s = (2\alpha+1)/(\alpha+1)$. The analysis of five AGN by Behar (2009) indicated values of $\alpha \simeq 0$–0.3, implying values of $s \simeq 1$–1.25. These values indicate that the ionization parameter $\xi(r) \propto r^{(2-s)}$ decreases with distance r from the accreting black hole, implying that the lower ionization species occur at larger distances and therefore have lower velocities. This indeed appears to be the case since we generally have $v(r) \propto r^{-1/2}$ in accretion/wind problems. The radial dependence of the wind column is then given by $N_H(r) \simeq r^0 - r^{-0.25}$, which is a rather slow variation that allows discernible absorption even for the lowest ξ ions.

Clearly, these scalings are very different from those expected for radiatively or thermally driven winds that are generally considered in AGN. The latter, which are driven from regions of limited extent but high luminosity L or temperature T, develop a radial density dependence steeper than $n(r) \propto r^{-2}$ as the wind accelerates with $n(r) \propto r^{-2}$ asymptotically, implying that the wind ionization increases with distance while the asymptotic column density $N_H(r) \propto r^{-1}$ decreases sufficiently fast to preclude a significant column for the ions forming at the largest distances (highest ξ ions). The winds uncovered by these ionization structure studies are obviously distinctly different from those reported by Tombesi et al. (2013) if they are to conform to the relations discussed above; in fact, they are consistent with the winds launched by the rotation of the magnetic fields that thread the AGN accretion disks across their full extent (Blandford and Payne, 1982; Contopoulos and Lovelace, 1994). These range from near the black hole to the length of its sphere of influence, namely, 10^5–$10^6 r_S \sim 1$ pc, i.e., out to the AGN tori; in fact, as proposed by Konigl and Kartje (1994), these MHD winds are the AGN tori. These winds are the solutions of the axisymmetric MHD equations under self-similar conditions, which is a reasonable assumption considering their great radial extent. Their power-law density scalings are a consequence of the self-similarity, along with their angular (poloidal) distribution given by the equation of transverse momentum balance or Grad–Safranov equation.

2.2.2 Wind ionization structure

Assuming a power-law radial wind density provided by the accretion disk MHD wind models of Contopoulos and Lovelace (1994), Fukumura et al. (2010a, 2010b) computed the ionization structures of the winds with the density parameter $s = 1$, i.e., $\alpha = 0$. The results of these calculations are shown in Figure 2B and depict the ionic columns of several Fe ions, namely, Fe XXV, Fe XVII, Fe XIII, and Fe III, as functions of ξ or r. It can be seen that while the distance of the maximum column among these ions increases with decreasing ionization state, the maximum value remains independent of r or ξ, in broad agreement with the data.

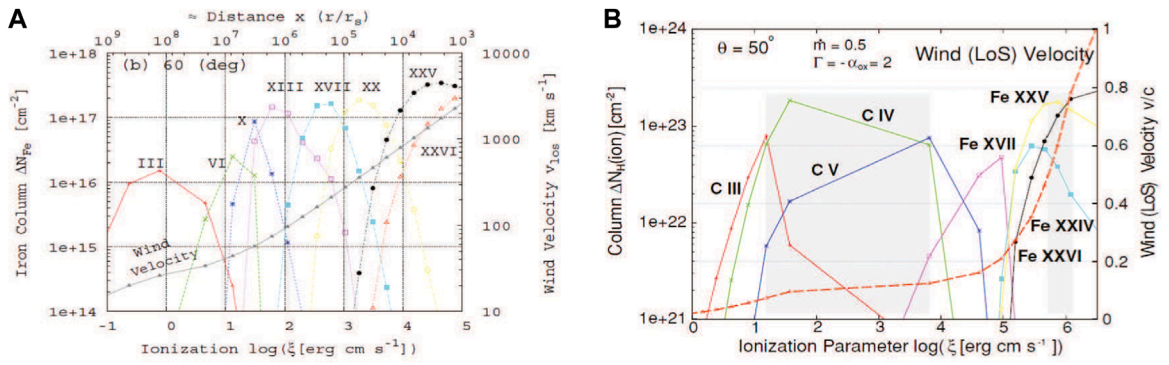

FIGURE 2
(A) Ionization structure of a wind having a density profile with $p = 1$ as a function of ξ and distance from the black hole. The wind velocity with distance r is given by the dashed line. **(B)** Ionization structure of the same wind but with an ionizing flux ×10 smaller. The shaded region indicates the ξ range over which C IV and C V can be found, showing that reduction of the ionizing flux can increase the outflow velocities.

Fukumura et al. (2010b) showed the ionization structures of these winds with the X-ray luminosity decreased relative to that of the BBB (which is used to set the normalizations of the accretion disk and wind densities at the inner disk edge, i.e., $x = 1$). The decrease in the ionizing flux (for a given density as a function of r) decreases the location of occurrence of a given ion, thus increasing its corresponding velocity. Hence, when all other conditions are equal, according to these considerations, the broad absorption line quasi-stellar objects (BAL QSOs) must be associated with the AGN of the reduced X-ray relative to the UV fluxes, a fact that is generally consistent with the observations.

To further test the notion that much of the absorber phenomenology can be accounted for by the photoionization of a given MHD outflow when given the ionizing luminosity, Fukumura et al. (2018) employed the same type of MHD wind model to derive a global fit to the data of the galactic X-ray binary GRO 1655-40, a source exhibiting blue-shifted features with high S/N ratio. In accordance with the proposed notion, because the bolometric source luminosity (including that of the quasithermal BBB component) is also the ionizing luminosity for black holes of $M \sim 10 M_\odot$, given the same value of the outflow Thomson depth τ as that of the AGN (τ is independent of the black hole mass), the outflow is fully ionized to a larger distance; as a result, ions with the highest ionizations, such Fe XXVI and Fe XXV, also occur at velocities of $v \sim 2{,}000$ km/s, while ions with lower ionizations like Ne X have velocities of only $v \sim 300$ km/s (Figure 3).

2.3 L_{UV}/L_X ratio

One of the most important consequences of the specific values of the wind density profiles $n(r)$ obtained by Behar (2009) and employed in the models of Fukumura et al. (2010a) is the wind mass flux, especially its radial dependence that is given in dimensionless units by

$$\frac{\dot{M}(x)}{\dot{M}_E} = \dot{m}(x) \simeq r_S\, n_0\, \sigma_T\, x^2 x^{-p} x^{-1/2} = \dot{m}_0 x^{3/2-p} = \dot{m}_0 x^{\beta} \qquad \beta = 3/2 - p. \tag{1}$$

It is interesting to note that for $p < 3/2$, the wind mass flux increases with distance from the black hole. This behavior implied by the absorber observations is allowed within the MHD disk wind approach of Contopoulos and Lovelace (1994) and is crucially related to the possibility of wind launching across the entire disk domain.

At the same time, the mass flux in the disk, i.e., its accretion rate, decreases toward the black hole, implying that the disk deviates from that of the standard SS73 (Tombesi et al., 2013; Luminari et al., 2020) and that the disk loses most of its available matter and angular momentum to the wind. This provides the possibility of converting the inner segments of the disk to an ADAF (Narayan and Yi, 1994) or rather an ADvection Inflow-Outflow Solutions (ADIOS) (Blandford and Begelman, 1999). As noted by Narayan and Yi (1994), this occurs when the local dimensionless accretion rate $\dot{m}(x) < \alpha^2$, where α is the (local) disk viscosity coefficient.

These considerations bring consistency to the picture of the X-ray binary disks as functions of their luminosities, as described in Esin et al. (1997, 1998); these authors conjectured the presence of an ADAF in the inner flow regions based on observations and that its size decreased with increasing luminosity, i.e., with increasing $\dot{m}$. Equation (1) then implies that there is a transition radius at $x = x_{tr}$ such that

$$\dot{m}_0 x_{tr}^{\beta} = \alpha^2, \quad \text{or} \quad x_{tr} = \left(\frac{\alpha^2}{\dot{m}_0}\right)^{1/\beta} \tag{2}$$

and that for $x > x_{tr}$, the disk geometry is that of the standard black body emitting accretion disk of luminosity L_{UV}; here, we assume an AGN of sufficiently large black hole mass to emit in the UV. However, for $x < x_{tr}$, the disk geometry is that of the geometrically thick hot ADAF/ADIOS, which is the main source of X-ray emission. It is worth noting that such a geometry is supported by recent X-ray polarimetric observations (Krawczynski et al., 2022; Gianolli et al., 2023; Tagliacozzo et al., 2023). These considerations then allow separate computations of the quasithermal viscous disk emission and X-ray emission by accounting for the efficiency of the hot/ADAF being proportional to $\dot{m}(x)$ and the presence of an inner edge to this disk segment at the ISCO of $x = x_0 \simeq 1$ (depending on the value of the black hole spin), which limits its efficiency; it is assumed that

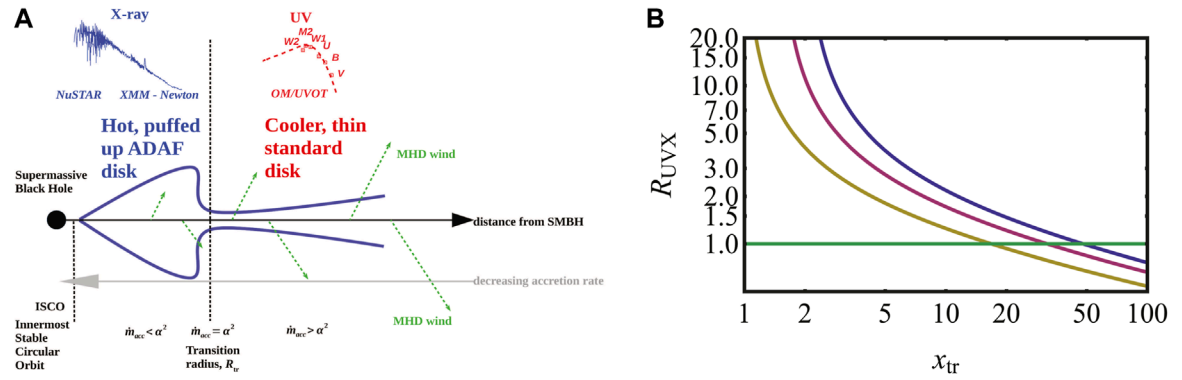

FIGURE 3
(A) Schematic depiction of the accretion geometry: the viscous disk of radially decreasing accretion rate converts to an ADAF at a transition radius of x_{tr} given by Eq. (2). The ADAF segment produces hard X-rays, while the thin disk segment produces UV-optical emissions. **(B)** Ratio $R_{UVX} = L_{UV}/L_X$ of the luminosities of the two segments across the transition radius x_{tr}. The different curves correspond to different values of x_0, which is the normalized ISCO radius. From top to bottom, the curves correspond to $x_0 = 2.0, 1.5,$ and 1.0.

there is no X-ray production in the free-falling segment of the flow interior to x_0. Under these conditions, the following expressions are obtained for L_{UV} and L_X.

$$L_X \propto \int_{x_0}^{x_{tr}} \frac{\dot{m}(x)^2}{x^3}\left[1-\left(\frac{x_0}{x}\right)^{1/2}\right]xdx, \quad (3)$$

$$L_{UV} \propto \int_{x_{tr}}^{\infty} \frac{\dot{m}(x)}{x^3}xdx, \quad (4)$$

It should be noted that the ration of the quantities of Eqs 3, 4, $R_{UVX} = L_{UV}/L_X$, depends mainly on the dimensionless accretion rate $\dot{m}_0$ and value of x_{tr} given by Eq. (2). It should also be noted that for a sufficiently large value of $\dot{m}_0$, L_X can nominally vanish as the X-ray emitting disk segment $[x_0, x_{tr}]$ is "squeezed" to near zero. This notion is consistent with statements on recent observations of the X-ray transient source MAXI J1820 + 070, whose corona contracted as the source luminosity increased (Kara et al., 2018).

According to the proposed notion, the general fact is that for bright AGN, $L_{UV} > L_X$ is indicative of the dimensionless accretion rates. On the other hand, at sufficiently low values of $\dot{m}_0$, the X-ray luminosities may be comparable to those of the thermal components, indicating a value close to fifty for x_{tr}, as shown in Figure 3.

Figure 3A presents a schematic representation of the disk structure including the standard and ADAF components along with the corresponding spectra of each segment. Their given shapes are only indicative and can be calculated more accurately if the size of the X-ray region is given along with the electron heating rates.

3 Discussion: timing implications

We present a global perspective of the AGN physics and resulting SED components within the framework of a single parameter, namely, the dimensionless accretion rate. It should be noted that the single most important feature of this entire scheme is the radial decrease of the disk accretion rate effected by the MHD winds launched across the entire disk domain. These apparently remove and eject most of the mass available for accretion onto the black hole (along with the angular momentum) to infinity to provide the observed phenomenology of the X-ray emission, BBB, and FIR molecular tori. It is important to note that within the present framework, these components are not independent but related via the same global MHD winds that extend over six decades in terms of radius. The X-ray absorber observations and their corresponding wide *xi* ranges are crucial for developing and establishing this notion, which help determine the dependence of their density on distance from the black hole through the AMD.

The wide radial ranges of these winds also imply a very wide range of the AGN time-domain properties. Unfortunately, human limitations cannot capture the entire range of AGN variations. In this respect, the scale invariance of the column densities allows scaling of the variability studies of accreting galactic black holes to the properties of the AGN brethren. As much as this scaling may be reasonable, it is not clear to this author that such an extrapolation would indeed be valid. However, time-domain studies that could even refute such scaling would be invaluable in probing the physics underlying the accretion dynamics.

Time reverberation studies by Kara et al. (2021) and the references therein have provided much information for probing the near-black-hole geometry. Despite much efforts, the preferred model of a lamppost over a thin viscous disk cannot reproduce the entire phenomenology. The picture of the accretion flow given in Figure 3 along with the underlying physics of the radially variable accretion rate may provide novel insights on the geometries and physics to be tested with this technique.

Finally, the tidal disruption of stars by the AGN black holes (Chan et al., 2019 and references therein) can lead to interesting phenomena that could provide additional tests to the above picture. First of all, a stellar disruption will provide additional mass for accretion and also ejection. In either case, one can expect novel phenomena: higher accretion rates should modify the SEDs, while ejection of matter through the winds of roughly constant columns should have different observables if launched in vacuum. Of great interest here would be the variation of the properties of the absorbers following such an event (Pasham et al., 2024). Sufficient sensitivity and spectral resolution will also enable

mapping of the interaction phase space along the LoS of the observer. Furthermore, studies on the line emission properties will offer a broader picture of the results of such interactions. The future of time-domain studies thus looks very promising.

Author contributions

DK: writing–original draft and writing–review and editing.

Funding

The author(s) declare that no financial support was received for the research, authorship, and/or publication of this article.

Acknowledgments

The author would like to thank his collaborators in this enterprise E. Behar, I. Contopoulos, K. Fukumura, C. Shrader, and P. Tzanavaris for their many insights, comments, and discussions on the AGN wind issues over the past several years.

Conflict of interest

The author declares that the research was conducted in the absence of any commercial or financial relationships that could be construed as a potential conflict of interest.

Publisher's note

References

Antonucci, R. (1993). Unified models for active galactic nuclei and quasars. *jnlARA&A* 31, 473–521. doi:10.1146/annurev.aa.31.090193.002353

Behar, E. (2009). Density profiles in seyfert outflows. *jnlApJ* 703, 1346–1351. doi:10.1088/0004-637X/703/2/1346

Blandford, R. D., and Begelman, M. C. (1999). On the fate of gas accreting at a low rate on to a black hole. *jnlMNRAS* 303, L1–L5. doi:10.1046/j.1365-8711.1999.02358.x

Blandford, R. D., and Payne, D. G. (1982). Hydromagnetic flows from accretion discs and the production of radio jets. *jnlMNRAS* 199, 883–903. doi:10.1093/mnras/199.4.883

Boroson, T. A. (2002). Black hole mass and Eddington ratio as drivers for the observable properties of radio-loud and radio-quiet QSOs. *jnlApJ* 565, 78–85. doi:10.1086/324486

Chan, C.-H., Piran, T., Krolik, J. H., and Saban, D. (2019). Tidal disruption events in active galactic nuclei. *jnlApJ* 881, 113. doi:10.3847/1538-4357/ab2b40

Contopoulos, J., and Lovelace, R. V. E. (1994). Magnetically driven jets and winds: exact solutions. *jnlApJ* 429, 139. doi:10.1086/174307

Crenshaw, D. M., Kraemer, S. B., and George, I. M. (2003). Mass loss from the nuclei of active galaxies. *jnlARA&A* 41, 117–167. doi:10.1146/annurev.astro.41.082801.100328

Esin, A. A., McClintock, J. E., and Narayan, R. (1997). Advection-dominated accretion and the spectral states of black hole X-ray binaries: application to nova muscae 1991. *jnlApJ* 489, 865–889. doi:10.1086/304829

Esin, A. A., Narayan, R., Cui, W., Grove, J. E., and Zhang, S.-N. (1998). Spectral transitions in Cygnus X-1 and other black hole X-ray binaries. *jnlApJ* 505, 854–868. doi:10.1086/306186

Frank, J., King, A., and Raine, J. (1985) *Accretion power in Astrophysics*. New York: Cambridge University Press.

Fukumura, K., Kazanas, D., Contopoulos, I., and Behar, E. (2010a). Magnetohydrodynamic accretion disk winds as X-ray absorbers in active galactic nuclei. *jnlApJ* 715, 636–650. doi:10.1088/0004-637X/715/1/636

Fukumura, K., Kazanas, D., Contopoulos, I., and Behar, E. (2010b). Modeling high-velocity QSO absorbers with photoionized magnetohydrodynamic disk winds. *jnlApJ* 723, L228–L232. doi:10.1088/2041-8205/723/2/L228

Fukumura, K., Kazanas, D., Shrader, C., Behar, E., Tombesi, F., and Contopoulos, I. (2018). Magnetized disk winds in NGC 3783. *jnlApJ* 853, 40. doi:10.3847/1538-4357/aaa3f6

Holczer, T., Behar, E., and Kaspi, S. (2007). Absorption measure distribution of the outflow in IRAS 13349+2438: direct observation of thermal instability? *jnlApJ* 663, 799–807. doi:10.1086/518416

Kara, E., Dai, L., Reynolds, C. S., and Kallman, T. (2018). Ultrafast outflow in tidal disruption event ASASSN-14li. *jnlMNRAS* 474, 3593–3598. doi:10.1093/mnras/stx3004

Kara, E., Mehdipour, M., Kriss, G. A., Cackett, E. M., Arav, N., Barth, A. J., et al. (2021). Agn storm 2. I. First results: a change in the weather of mrk 817. *jnlApJ* 922, 151. doi:10.3847/1538-4357/ac2159

Kazanas, D., Fukumura, K., Behar, E., Contopoulos, I., and Shrader, C. (2012). Toward a unified AGN structure. *Astronomical Rev.* 7, 92–123. doi:10.1080/21672857.2012.11519707

Konigl, A., and Kartje, J. F. (1994). Disk-driven hydromagnetic winds as a key ingredient of active galactic nuclei unification schemes. *jnlApJ* 434, 446. doi:10.1086/174746

Lynden-Bell, D. (1969). Galactic nuclei as collapsed old quasars. *jnlNature* 223, 690–694. doi:10.1038/223690a0

Morgan, C. W., Kochanek, C. S., Morgan, N. D., and Falco, E. E. (2010). The quasar accretion disk size-black hole mass relation. *jnlApJ* 712, 1129–1136. doi:10.1088/0004-637X/712/2/1129

Narayan, R., and Yi, I. (1994). Advection-dominated accretion: a self-similar solution. *jnlApJ* 428, L13. doi:10.1086/187381

Netzer, H. (2015). Revisiting the unified model of active galactic nuclei. *jnlARA&A* 53, 365–408. doi:10.1146/annurev-astro-082214-122302

Novikov, I. D., and Thorne, K. S. (1973). Astrophysics of black holes. *Black Holes Les. Astres Occlus*, 343–450.

Reynolds, C. S., and Fabian, A. C. (1995). Warm absorbers in active galactic nuclei. *jnlMNRAS* 273, 1167–1176. doi:10.1093/mnras/273.4.1167

Shakura, N. I., and Sunyaev, R. A. (1973). Black holes in binary systems. Observational appearance. *jnlA&A* 24, 337–355.

Shapiro, S. L., and Teukolsky, S. A. (1986) *Black holes, white Dwarfs and neutron stars: the Physics of compact objects (willey and sons)*.

Strateva, I. V., Brandt, W. N., Schneider, D. P., Vanden Berk, D. G., and Vignali, C. (2005). Soft X-ray and ultraviolet emission relations in optically selected AGN samples. *jnlAJ* 130, 387–405. doi:10.1086/431247

Sulentic, J. W., del Olmo, A., Marziani, P., Martínez-Carballo, M. A., D'Onofrio, M., Dultzin, D., et al. (2017). What does CIVλ1549 tell us about the physical driver of the Eigenvector quasar sequence? *jnlA&A* 608, A122. doi:10.1051/0004-6361/201630309

Sulentic, J. W., Marziani, P., and Dultzin-Hacyan, D. (2000). Phenomenology of broad emission lines in active galactic nuclei. *jnlARA&A* 38, 521–571. doi:10.1146/annurev.astro.38.1.521

Tombesi, F., Cappi, M., Reeves, J. N., Palumbo, G. G. C., Yaqoob, T., Braito, V., et al. (2010). Evidence for ultra-fast outflows in radio-quiet AGNs: I. Detection and statistical incidence of Fe K-shell absorption lines. *jnlA&A* 521, A57. doi:10.1051/0004-6361/200913440

Urry, C. M., and Padovani, P. (1995). Unified schemes for radio-loud active galactic nuclei. *jnlPASP* 107, 803. doi:10.1086/133630